Available online at www.sciencedirect.com

SCIENCE DIRECT®

Inorganica Chimica Acta 349 (2003) 217–226

Inorganica Chimica Acta

www.elsevier.com/locate/ica

Effect of ZrO_2 content on textural and structural properties of CeO_2–ZrO_2 solid solutions made by citrate complexation route

J. Kaspar[a,*], P. Fornasiero[a], G. Balducci[a], R. Di Monte[a], N. Hickey[a], V. Sergo[b]

[a] *Dipartimento di Scienze Chimiche, Università di Trieste, via L. Giorgieri 1, I-34127 Trieste, Italy*
[b] *Dipartimento di Ingegneria dei Materiali e Chimica Applicata, Università di Trieste, Via Valerio 2, I-34127 Trieste, Italy*

Received 15 July 2002; accepted 19 September 2002

Dedicated to Professor Mauro Graziani on his 65th birthday.

Abstract

Single phase homogeneous CeO_2–ZrO_2 solid solutions with various compositions were synthesized using a citrate complexation route. Investigation of the sintering behaviour disclosed important modifications of the textural and, in particular, structural properties, which apparently create a strongly defective structure that could explain the unusual redox properties of these catalytic systems.

© 2003 Elsevier Science B.V. All rights reserved.

Keywords: Exhaust catalysts; CeO_2–ZrO_2 solid solution; CeO_2–ZrO_2; Synthesis of mixed oxides

1. Introduction

Synthesis of new catalytic nanophase materials is attracting strong interest since it has been shown that by tuning the structural and textural properties of an active component on a nanoscale level, quantum size effects may become important, leading to new and unpredicted chemical and catalytic properties [1]. This is efficiently illustrated by the case of oxide-supported gold systems. This metal was traditionally considered catalytically inactive, given its inability to chemisorb small molecules such as CO, H_2, etc. [2], until Haruta et al. [3] identified an unexpectedly high activity of a Au/Fe_2O_3 catalyst in CO oxidation at very low temperature (203 K). The origin of this high activity has been attributed to various factors (preparation methods, nature of the support and pre-treatment, morphology of the gold particles), however, the crucial point is that all of these factors lead to a nanometer sized dispersion of the supported gold particles, the maximum activity being observed for particles with a diameter of 2–3 nm [3,4].

$Ce_xZr_{1-x}O_2$ mixed oxides have a number of important catalytic applications: they are extensively employed in current automotive three-way catalysts (TWC) as the oxygen storage promoters, i.e. materials that regulate the oxygen partial pressure through the Ce^{3+}/Ce^{4+} redox couple, thereby keeping the oxidants-to-reductants ratio in the exhaust at the stoichiometric value where the highest pollutant conversions are attained [5]. They exhibit high thermal stability compared to the traditionally employed CeO_2, as well as an exceptional ability to promote the catalytic activity of supported noble metals (NM) with respect to conventional supports, such as Al_2O_3 or SiO_2, and even with respect to CeO_2 itself [6]. Similar advantages of the use of $Ce_xZr_{1-x}O_2$ as NM support have been identified in a wide range of applications in the fields of chemicals, energy production (reformer/WGSR in on-board H_2 production for fuel cell, catalytic combustion), catalysts for abatement of pollutants, etc. [7,8]. Despite their apparent simplicity, at least in terms of chemical composition, these materials show rather intriguing properties. In particular, their redox behaviour, on which their main function in TWCs is based, has been shown to depend on several factors, including structure [9], texture [10,11], phase homogeneity [12] and even the

---

[*] Corresponding author. Fax: +39-040-558 3903.
E-mail address: kaspar@units.it (J. Kaspar).

0020-1693/03/$ - see front matter © 2003 Elsevier Science B.V. All rights reserved.
doi:10.1016/S0020-1693(03)00034-3

pre-treatment [13–16]. A variety of methodologies have been applied to the synthesis of $Ce_xZr_{1-x}O_2$ [17], however, despite the large amount of work, a number of fundamental questions related to these systems, such as which is the optimal $Ce_xZr_{1-x}O_2$ composition in terms of redox and textural stability, still remain open. A possible interpretation of such variability in their chemical behaviour is that, due to limited solubility of ZrO_2 in the CeO_2 lattice, metastable phases and domain-type structures may be formed at a nanoscale level in the synthesis, which cannot be easily detected by conventional characterisation methods [18]. Failure to detect such inhomogeneities would effectively result in comparison of different materials with nominally equal composition. Co-precipitation and gel-like synthesis methods indeed often lead to compositionally inhomogeneous mixed oxides [19,20]. Accordingly, contradictory results have been reported in the literature on what should be the best $Ce_xZr_{1-x}O_2$ composition in terms of thermal stability and redox properties: either CeO_2- or ZrO_2-rich, or even $Ce_{0.5}Zr_{0.5}O_2$, have all been indicated as the most effective compositions [10,21,22]. Furthermore, remarkably different textural and chemical behaviour can be achieved by tuning the synthesis method at a single sample composition ($Ce_{0.2}Zr_{0.8}O_2$) [23]. Evidently, a single synthesis method, reproducibly leading to homogeneous solid solutions, is needed to truly assess the effects of the $Ce_xZr_{1-x}O_2$ composition. In this work, a citrate complexation synthesis method is applied to investigate the effects of $Ce_xZr_{1-x}O_2$ composition on structural and textural properties. The aim is that of using a single synthesis methodology which allows production of compositionally homogeneous systems across the whole $Ce_xZr_{1-x}O_2$ range of compositions, as it has been shown previously the applicability of such method for selected compositions, even though single phase systems were not always obtained [24]. It is shown here that the citrate route using water as solvent can be conveniently employed to obtain homogeneous single phase products over a wide compositional range.

2. Experimental

$Ce_xZr_{1-x}O_2$ ($x = 0.2$, 0.4, 0,5, 0.6, 0.8) solid solutions and pure cerium and zirconium oxides were synthesised from nitrate precursors by complexing the metal cations with the citrate [25]. The preparation was carried out as follows. After dissolving $Ce(NO_3)_3{\cdot}6H_2O$ (32.1% Ce, Aldrich) and $ZrO(NO_3)_2{\cdot}nH_2O$ (27.32% Zr, Aldrich) in H_2O, a solution of citric acid (99.7%, Prolabo) in H_2O was added, leading to a final concentration of mixed oxide of 40 $g\,l^{-1}$. The resulting solution was stirred at 353 K for 2.5 h to obtain a complete dissolution of the precursors and then at room temperature (r.t.) for at least 12 h. The solvent was subsequently eliminated on a rotary evaporator. First, a transparent gel was obtained and then, after the evolution of nitrogen oxides, a solid was recovered. This was heated in air from r.t. to 773 K at a rate of 3 K min^{-1} and calcined at this temperature for 5 h. Henceforth, these samples are indicated as fresh. Effects of calcination (5 h) were investigated in the temperature range from 873 to 1273 K. N_2 adsorption isotherms at 77 K were measured on a Micromeritics ASAP 2000 analyser.

Raman spectra were obtained on either a Perkin-Elmer 2000 FT-Raman spectrometer with a diode pumped YAG laser (1064 nm) and a r.t. super InGaAs detector, using a laser power of 200 or 600 mW; or a Renishaw S1000 system with an Ar^+ ion laser (514.5 nm) operating in the back scattering geometry. In this latter case the power delivered to the sample was about 5 mW.

SEM micrographs were taken with a conventional scanning electron microscope (Cambridge Inc.). Before taking the images the powders were dispersed in water, a drop of the suspension was deposited onto the specimen holder and, after water evaporation, the powder was coated with gold to prevent charging under the electron beam.

Powder X-ray diffraction patterns were collected on a Siemens Kristalloflex Mod.F diffractometer using Ni-filtered Cu Kα. The particle sizes of the powdered samples were calculated from the diffraction patterns using the Schrerrer formula [26].

3. Results and discussion

The use of citric acid as complexing agent, employed as described in Section 2, leads to formation of apparently homogeneous gel-like materials at all the compositions investigated. These materials were then dried and calcined to obtain white (ZrO_2) to yellow (CeO_2) powders, which were characterized by different techniques to assess the following aspects: (i) homogeneity of the mixed oxide, (ii) effects of increasing calcination temperature on structural and (iii) textural stability.

3.1. XRD and Raman characterization

Before discussing the results, let us recall some features of the $Ce_xZr_{1-x}O_2$ phase diagram. CeO_2 crystallizes in the fluorite structure (space group $Fm\bar{3}m$), while ZrO_2 is monoclinic at r.t. (space group $P2_1/c$). Given the relatively large difference (13%) between the cation radii of Ce^{4+}(0.097 nm) and Zr^{4+} (0.084 nm), a limited mutual solubility might be expected [27]. Consistently, only the tetragonal (t-) and cubic (c-)phases, found respectively at high (>80 mol.%) and low (<20 mol.%) ZrO_2 contents, are thermodynamically stable, while two metastable tetragonal phases (t', t'') may be formed at intermediate compositions [28]. The presence of metastable phases poses serious difficulties to researchers—sometimes underestimated—regarding assessment of the homogeneity of the prepared solid solution. Vegard's rule is typically applied for this purpose. Due to the lower cation radius of Zr(IV) compared to Ce(IV), a linear decrease of the cell parameter (or cell volume, when t-phases are included) is expected and, in fact, observed [29,30]. However, the as-synthesized high surface area samples typically feature quite broad XRD peaks, due to the nanometer dimension of the crystallites. This does not allow an unambiguous detection of a single phase product. After calcination 1073–1273 K for 2–5 h, significant sharpening of the XRD patterns is normally observed, which is due to the growth and sintering of the crystallites. However, such sintering often leads to the appearance of strongly asymmetric peaks in the XRD spectra, which has been attributed to metastable nature of the $Ce_xZr_{1-x}O_2$ of intermediate compositions, leading to phase segregation upon calcination at high temperature [31,32]. In principle, the metastable nature of these mixed oxides makes assessment of structural homogeneity difficult.

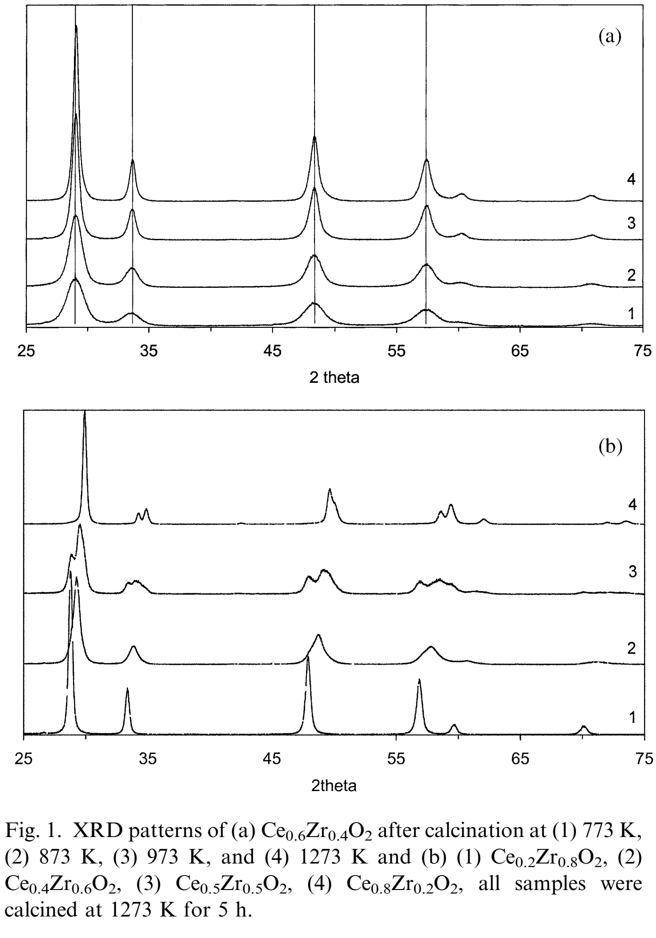

Fig. 1. XRD patterns of (a) $Ce_{0.6}Zr_{0.4}O_2$ after calcination at (1) 773 K, (2) 873 K, (3) 973 K, and (4) 1273 K and (b) (1) $Ce_{0.2}Zr_{0.8}O_2$, (2) $Ce_{0.4}Zr_{0.6}O_2$, (3) $Ce_{0.5}Zr_{0.5}O_2$, (4) $Ce_{0.8}Zr_{0.2}O_2$, all samples were calcined at 1273 K for 5 h.

The evolution of the powder XRD patterns with increasing temperature of calcination was therefore investigated. Typical results are exemplified in Fig. 1(a) for $Ce_{0.6}Zr_{0.4}O_2$. The fresh sample features broad, symmetric XRD peaks which strongly sharpen as the calcination temperature increases. In the range investigated, no evidence indicated that phase segregation could be induced by the increase of the calcination temperature up to 1273 K. This is an important point since in our previous investigation of such composition, evidence for phase inhomogeneity, revealed by asymmetric peak profiles, was detected [24]. We observed that, as indicated in Section 2, a complete dissolution of the precursors must be ensured in the synthesis to obtain phase homogeneity. In fact, we have used water as solvent in this work instead of methanol [24]. Similar symmetrical XRD patterns are observed after calcination at 1273 K in the cases of the other compositions (Fig. 1(b)), except for the $Ce_{0.4}Zr_{0.6}O_2$ and ZrO_2 samples (the latter sample is not reported). In the former case, phase segregation into a CeO_2-rich and ZrO_2-rich mixture was detected for calcination temperatures at and above 973 K, whilst in the latter case, transformation of t-ZrO_2 into m-ZrO_2 with increasing calcination temperatures was detected.

Except in the above quoted cases for high calcination temperatures, and to some extent for the $Ce_{0.2}Zr_{0.8}O_2$ sample (see below), Vegard's rule is nicely followed by all the compositions here investigated (Fig. 2). This is an important finding that indicates the versatility of the present synthesis method for obtaining single phase solid solutions (to the detection limit of the XRD technique) for a wide interval of $Ce_xZr_{1-x}O_2$ compositions. For comparison, by the usual co-precipitation techniques, single phase solid solutions could not be obtained over a large compositional range, even for commercial products [33,34]. The data shown in Fig. 2

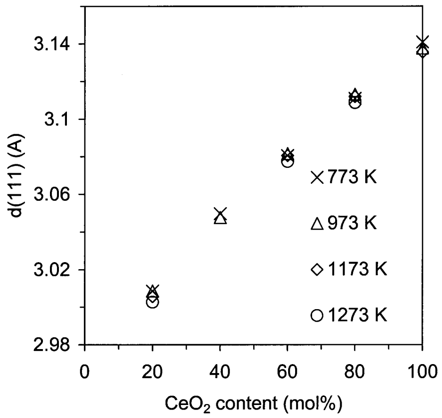

Fig. 2. Vegard rule for the $Ce_xZr_{1-x}O_2$ ($x = 0.2$, 0.4, 0.6, 0.8) solid solutions and CeO_2 detected as variation of d(1 1 1) with CeO_2 content for samples calcined at the indicated temperatures. Pseudocubic cell is considered for the tetragonal samples.

suggest that the phase segregation observed at high temperatures for $Ce_{0.4}Zr_{0.6}O_2$ should preferably be attributed to a high tendency of this composition to segregate, due to existence of a bi-phasic (t and t') region in the phase diagram around this composition [35], rather than to the formation of compositional inhomogeneities in the synthesis [12]. The deviation from the linearity observed for d(1 1 1) in the case of $Ce_{0.2}Zr_{0.8}O_2$ is attributed to the fact that there is a significant tetragonal distortion of the pseudo-cubic unit cell with a ratio of $c/a = 1.017$. Rietveld fitting performed on the sample calcined at 1273 K confirmed the presence of a single phase product.

A perusal of Fig. 1(a) reveals, however, that there is a small but continuous shift of the XRD peaks to higher values of 2θ with increasing calcination temperature. Similar behaviour was also observed for the other compositions, except ZrO_2 and $Ce_{0.4}Zr_{0.6}O_2$ (vide supra). Rietveld analysis of the XRD patterns reported in Fig. 1(a) revealed a contraction of the cell volume from 0.15119 to 0.14919 nm^3 as the calcination temperatures was increased from 773 to 1273 K, corresponding to a relative decrease of 1.3%. Phase segregation in the $Ce_xZr_{1-x}O_2$ systems leads to CeO_2- and ZrO_2-rich phases; accordingly, if we assume that segregation of pure CeO_2 occurred, then segregation of about 5 wt.% of CeO_2 can be calculated for the above quoted variation of unit cell volume, which should have been detected under our experimental conditions. A further consideration is that an interpretation of this phenomenon in terms of phase segregation cannot be applied to CeO_2, as in fact a perusal of Fig. 2 indeed reveals some change of the lattice parameter also in this case. A possible interpretation is to relate these shifts to the nanometer particle size of the present catalysts: by decreasing the size of the particle, the ratio of surface to bulk atoms, which favours conversion of Ce(IV) to Ce(III) near the surface region [36], increases. This in turn leads to lattice expansion due to the higher ionic radius of Ce^{3+} compared to Ce^{4+} [37]. In our case obviously the opposite will occur. The reasons for such changes may be understood by considering that the standard potential for reduction of Ce^{4+} to Ce^{3+} is 1.74 V in solution [38], which indicates that Ce(IV) in solution is a strong oxidant. In the solid state, the situation is different. CeO_2 crystallises in the fluorite structure in which each cerium ion is co-ordinated by eight oxygen neighbours. This co-ordination stabilises the Ce^{4+} state and makes the reduction of CeO_2 unfavourable. In fact, the fluorite structure of ceria is a direct result of the ionic nature of ceria and of the charge and size of the ions. Model calculation has shown that it is formed when a sufficiently high number of CeO_2 units (~ 50) are clustered together [39].

On the other hand, expansion of the CeO_2 lattice parameter was observed for particle dimensions that are even smaller then those here observed [36], suggesting that some other subtle changes of the structural properties may also occur in the mixed oxides with increasing calcination temperature (see below).

Phase attribution and sample modification induced by the calcination were therefore investigated by Raman spectroscopy in the range 100–1000 cm^{-1}, where the absorption due to the M–O stretching is observed (Fig. 3). Six Raman-active modes of $A_{1g}+3E_g+2B_{1g}$ symmetry are observed for tetragonal ZrO_2 (space group $P4_2/nmc$), while for the cubic fluorite structure (space group $Fm\bar{3}m$) only one F_{2g} mode centred at around 490 cm^{-1} is Raman-active [40]. In pure CeO_2 ($Fm\bar{3}m$ space group), the F_{2g} mode is observed at 465 cm^{-1}.

The Raman spectra reported in Fig. 3 show the following features: (i) for CeO_2 contents of 100 and 80 mol.%, the spectrum is dominated by a single strong band which shifts to higher frequencies and becomes less sharp at lower CeO_2 content. This band is attributed to the F_{2g} mode. A minor peak at about 145 cm^{-1} is also present in the spectrum of $Ce_{0.8}Zr_{0.2}O_2$; (ii) at high ZrO_2 content ($\geqslant 80$ mol.%) five of the six bands of the tetragonal ZrO_2 are detected, while the presence of the monoclinic phase in clearly detected for the pure ZrO_2. Finally, (iii), at intermediate CeO_2 contents (40–60 mol.%), the spectrum is dominated by a broad and intense band at 530–540 cm^{-1} with shoulder at about 470 cm^{-1}. A weak band at about 125 cm^{-1} is also present.

The shift of the F_{2g} Raman frequency in $Ce_{0.8}Zr_{0.2}O_2$ to higher values with respect to CeO_2 is due to the decrease of the lattice parameter, resulting in shorter M–O bond lengths. The presence of the very weak feature at 145 cm^{-1} may suggest the presence of the t''-phase, i.e. a tetragonal (space group $P4_2/nmc$) phase with some distortion of the oxygen sublattice with respect to the cubic fluorite structure and with a ratio of unit cell parameters $c/a = 1$ [28]. For high ZrO_2 content, the spectral features are consistent with an essentially regular tetragonal $P4_2/nmc$ symmetry, with respectively short and long $M–O_I$ and $M–O_{II}$ bond distances. Among the six characteristic Raman modes of t-ZrO_2, the band at approximately 260 cm^{-1} corresponds to the stretching of $M–O_{II}$ and those at 610 and 640 cm^{-1} to that of $M–O_I$ [41]. Accordingly, when the amount of CeO_2 inserted into the ZrO_2 lattice is increased from 12 to 24 mol.%, the bands at 610 and 640 cm^{-1}, related to the stretching modes, shift and tend to overlap [42]. This accounts for the observation of five bands in the $Ce_{0.2}Zr_{0.8}O_2$ instead of the predicted six modes.

The observation of a few Raman modes with the strong features at 520–540 cm^{-1} for the intermediate CeO_2 contents cannot be easily rationalised on the basis of the proposed phase symmetries ($P4_2/nmc$ and $Fm\bar{3}m$) and the possible shifts of the stretching modes. More-

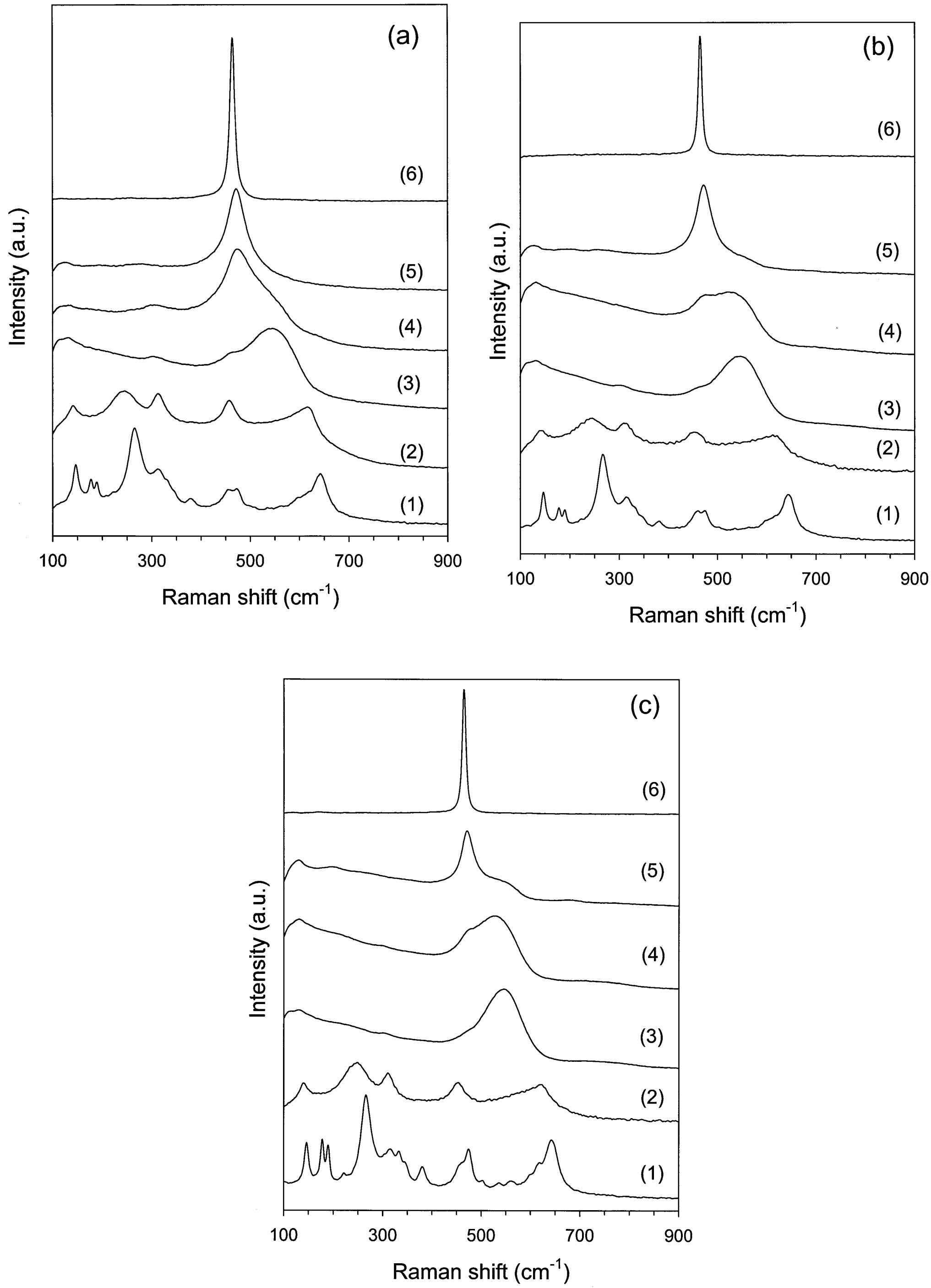

Fig. 3. Raman spectra of samples calcined at 773 K (a), 973 K (b) and 1173 K (c): ZrO_2 (1); $Ce_{0.2}Zr_{0.8}O_2$ (2); $Ce_{0.4}Zr_{0.6}O_2$ (3); $Ce_{0.6}Zr_{0.4}O_2$ (4); $Ce_{0.8}Zr_{0.2}O_2$ (5); CeO_2 (6) (laser power 200 mW).

over, the appearance of the spectra clearly changes with the temperature of calcination as detailed for $Ce_{0.6}Zr_{0.4}O_2$ in Fig. 4, suggesting the occurrence of some important changes in the structural properties of the sample. Such behaviour would not be expected from simple sintering. This aspect was further examined in some detail using different wavelength of the Raman excitation radiation (Fig. 4). A remarkable dependency of the Raman spectra on the excitation energy is clearly denoted by the presence of strong bands at 3360, 2490 and 1920 cm^{-1} that are observed only when IR excitation is used. The absence of the band at 525 cm^{-1} in the spectrum when the green light source is used is another noteworthy feature. The attribution of the band at 3360 cm^{-1} to surface OH groups is highly reasonable, substantiated also by the broad pattern of

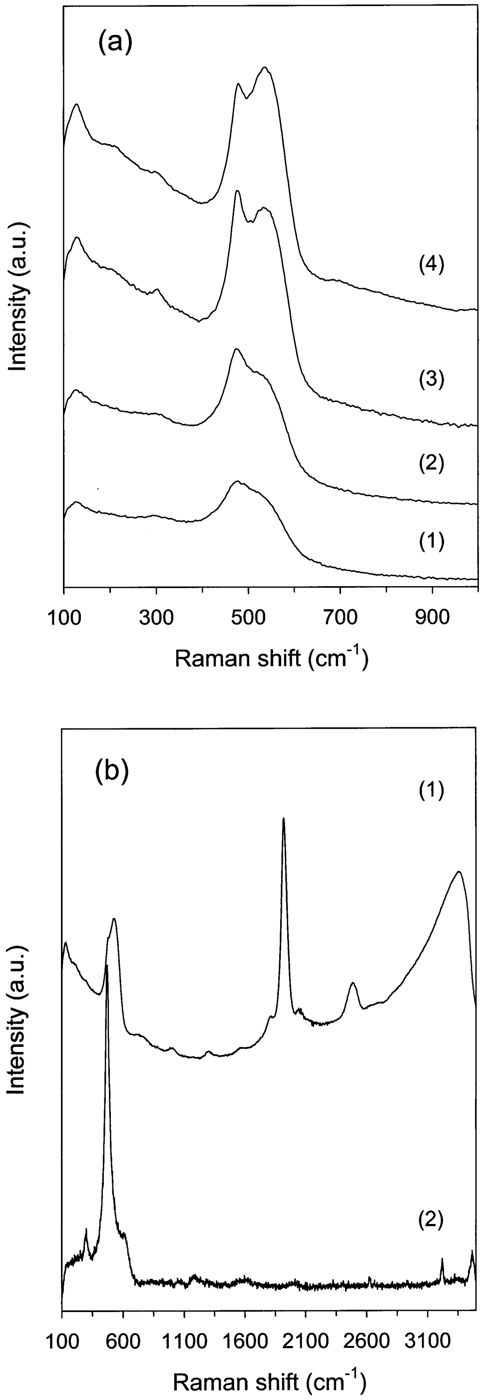

Fig. 4. Effect of calcination temperature (a) and Raman excitation line (b) on the spectra of $Ce_{0.6}Zr_{0.4}O_2$: (a) sample calcined at 773 K (1), 973 K (2), 1173 K (3) and 1273 K (4); (b) sample calcined at 1273 K, IR excitation at 1068 nm (laser power 600 mW) (1) and green light excitation at 514.5 nm (2).

the band. Conversely, the attribution of the bands at 2490, 1920 and 525 cm^{-1} is more uncertain. Generally speaking, the phonon spectra related to the M–O lattice are observed below 1000 cm^{-1}. Even though shifts in the phonon spectra due to introduction of foreign cation and, consequently, change of bond lengths can be detected in mixed fluorite oxides, they are relatively small and linearly related to the square root of the cell volume [41]. Thus, for the E_g mode that was found at 631 cm^{-1} in $Ce_{0.12}Zr_{0.88}O_2$ [43], we can estimate a value of 595 cm^{-1} for $Ce_{0.4}Zr_{0.6}O_2$ by applying the linear relationship found by Kim et al. for Y_2O_3 (2 mol.%)–CeO_2–ZrO_2 mixed oxides [41]. This is somewhat distant from the value of the peak maximum at 550 cm^{-1} observed in Fig. 3. On the other hand, it should be noted that the above relationship has been found to hold for the *t*-phase, whilst *t*′ or *t*″ phase are detected at CeO_2 content of 40–60 mol.%. It might be argued that the increase of the intensity of the band around 550 cm^{-1} could be related to a progressive tetragonalization of the lattice induced by the increase of the calcination temperature. This interpretation, however, is not supported by the Raman spectra obtained using the visible excitation line. In this case, the strong band around 550 cm^{-1} is not observed, the only apparent modification of the spectra with increasing calcination temperature being a sharpening of the peak with maximum at 466 cm^{-1} that shifts to 471 cm^{-1} (as the calcination temperature is increased from 973 to 1273 K). Note that, due to the nanometer dimension of the starting materials, this sharpening of the peak is fully consistent with the occurrence of particle sintering [44]. The shift to higher frequencies of the band at 466 cm^{-1}, attributed to the F_{2g} mode of the fluorite lattice, is consistent with the decrease of the lattice parameter observed by XRD. Generally speaking, decreasing the lattice parameter and hence cell volume, the lattice moves towards the structural features of the ZrO_2 systems and hence tetragonalization is expected, but it cannot explain the features due to the band at 530 cm^{-1}.

Another possibility is the band at 530 cm^{-1} could be attributed to luminescence, which accounts for its absence using the visible excitation [45]. However, even in this case, the variation of the relative intensity of the band at 530 and the shoulder at 465–478 cm^{-1} appears to be a clear indication of a subtle modification of the structure of the mixed oxide with increasing calcination temperature. Similar peak attribution could be also made for the bands at 1915 and 2500 cm^{-1}. None of these bands seems attributable to the presence of an impurity as their intensities relative to the peak/shoulder at about 470 cm^{-1} are neatly affected by the temperature of calcination in a similar fashion as the band around 530 cm^{-1}. No evidence for significant amounts of impurities was indeed found by X-ray fluorescence analysis of the sample.

It should be recalled that a band around 2100 cm^{-1} has been attributed to the $^2F_{7/2}\leftrightarrow{}^2F_{5/2}$ electronic transition of Ce^{3+} species in a reduced Y_2O_3 doped $Ce_xZr_{1-x}O_2$, and its intensity was related to the concentration of these species [46]. Formation of Ce^{3+} on calcination at high temperature and in the presence of oxygen might seem somewhat surprising but the presence of defects in $Ce_xZr_{1-x}O_2$ has long been recognized [47], even though their exact nature is still matter of debate [9,48]. Recently, Egami and coworkers suggested that the insertion of ZrO_2 in the CeO_2 lattice favours generation of Frenkel-type defects, the displacement of lattice oxygen to the octahedral sites possibly generating Ce^{3+} sites in the lattice [49]. These defects have been indicated as the origin of the mobility of the oxygen in the bulk of the $Ce_xZr_{1-x}O_2$ compared to CeO_2, leading to enhanced redox properties. Notice that a displacement of the oxygen atoms from the tetrahedral sites of the fluorite lattice into the octahedral ones could possibly lead to decrease of lattice parameter due to the larger size of the octahedral cavity.

An alternative view of such processes involving the generation of the Ce^{3+} species is to consider the removal of one electron from a doubly ionized oxygen vacancy to reduce Ce^{4+} to Ce^{3+} (defects in CeO_{2-x} are mainly doubly ionized vacancies, but the presence of singly ionized oxygen vacancies was recently detected in dynamically compacted m-ZrO_2 [50]); the standard enthalpy of this process in CeO_2 is 0.8–1 eV [51,52]. This energy corresponds to shift of about 2900–1300 cm^{-1} and 13 000–11 400 cm^{-1} relative to the IR and green excitation frequency, respectively. It is then quite reasonable to assume that the IR excitation frequency is much closer to a Raman resonant condition, with ensuing enhanced Raman efficiency for the bands which we observe in the range 1900–2500 cm^{-1} (Fig. 4). Usually excitation wavelengths far from Raman resonant conditions do not lead to a complete suppression of the bands: some intensity can still be recorded. In our case we do not observe the above quoted band at about 2100 cm^{-1}, but this can be due to very low concentration of the Raman resonant system or to low excitation power; indeed Otake et al. [46] did observe these bands in the ZrO_2–CeO_2–Y_2O_3 system, but they examine samples with much larger Ce^{3+} concentrations due to extremely low pO_2 (10^{-13}–10^{-19} Pa) using a laser power twice that of our case. Despite this, the intensity of the band at about 2100 cm^{-1} recorded by those authors is about 30 times weaker than in our case (as can be inferred from the relative intensity of this band with respect to the band at 470 cm^{-1} in our Fig. 4, and in their [46, Figs. 2 and 3]). In summary, we believe that the intense band at 1910 cm^{-1} is a resonant effect; as such it is coupled with an electronic transition close in energy to the peculiar IR excitation wavelength which gives rise to it. Even though the observed bands cannot be unequivocally assigned, a clear indication has been obtained, that is that the lattice structure and, more probably, the defect structure of the solid solution is strongly modified with increasing calcination temperature, particularly at the intermediate $Ce_xZr_{1-x}O_2$ compositions. There is therefore a striking difference between the pure CeO_2 and the ZrO_2-doped systems in that sintering leads to a highly ordered structure in the former case while disordered or defective lattice is created by the sintering of the $Ce_xZr_{1-x}O_2$, which can be attributed to the misfit between the Ce(IV) and Zr(IV) radii responsible for this lattice strain. This is observed as long as t''- and t'-, i.e. closely related to CeO_2, phases are considered, while for the t-$Ce_{0.2}Zr_{0.8}O_2$, whose structure is closely related to t-ZrO_2 we do not have evidence for such behaviour.

3.2. Textural and morphological characterization

Textural and morphological properties were investigated by N_2 physisorption, XRD and SEM techniques. The BET surface areas as a function of temperatures are reported in Fig. 5. Interestingly, at comparable synthesis conditions, there is a strong effect of the sample composition on the initial surface area, which is maximum at a CeO_2 content of 80 mol.%. The effect is quite remarkable as this sample features a BET surface area which is roughly three times that of either ceria or zirconia (64 vs. 18 and 20 $m^2\,g^{-1}$), indicating the favourable effect of the formation of the solid solution upon the textural properties. However, upon increasing the calcination temperature, due to the relatively poor textural stability that can be achieved by this synthesis methodology [23], the effects of the ZrO_2 addition become quite small in terms of the surface area measurements. Notwithstanding the relatively low and comparable BET areas, the retarding effects of the ZrO_2 addition on the rate of sintering are neatly detected by the XRD technique. The crystallite sizes were calculated from peak broadening using the Scherrer formula [26]. The data are reported in Fig. 6 and show that insertion of ZrO_2 into the CeO_2 lattice remarkably modifies the

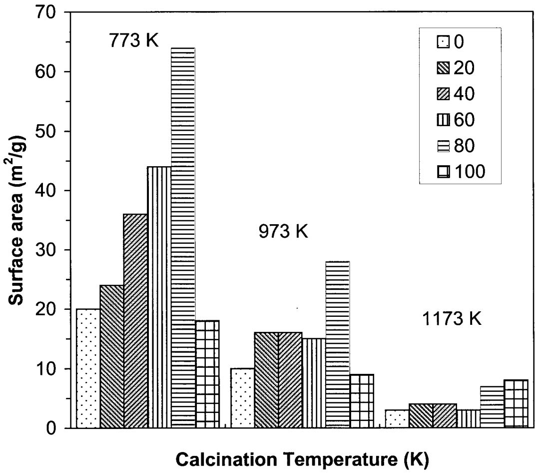

Fig. 5. Surface area measured by the BET method as a function of the calcination temperature (calcination temperatures and CeO_2 content are indicated).

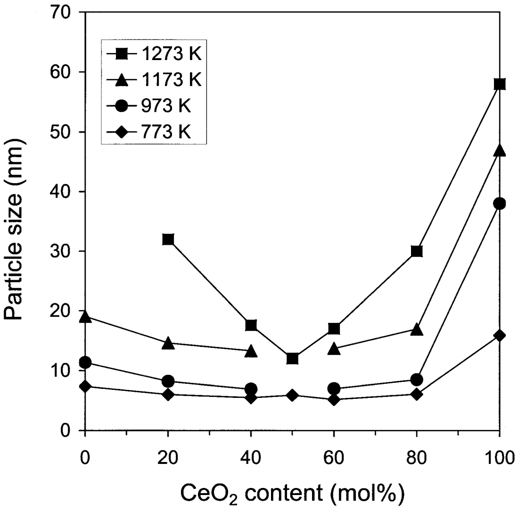

Fig. 6. Effect of ZrO_2 addition on the crystallite size after calcination at the indicated temperatures, as detected from the Schrerrer formula (average particle size is reported for ZrO_2 and $Ce_{0.4}Zr_{0.6}O_2$ when phase separation was detected).

sintering process of CeO_2. High ZrO_2 content significantly decreases the rate of sintering as long as the cubic or pseudo-cubic (t'') phase symmetry is maintained in the mixed oxide, leading to a pronounced minimum at intermediate composition, as shown by the data obtained after calcination at 1273 K. At this composition, reversible transition from the t'' to the t' phase was observed [28], leading to a highly defective system. The presence of this particular structure seems to be responsible for the unusually low sintering rate of this sample. It should be noted that, due to the high homogeneity of the initial precursor, no phase separation occurred under our calcination as checked by Rietveld analysis of the sample calcined at 1273 K. XRD line broadening, leading to apparent low particles size, is indeed observed when such segregation occurs [53]. Even though other factors, such as strain effects induced by the defective structure of local compositional inhomogeneities could in principle contribute to XRD line broadening, we believe that such factors should not significantly affect the present measurements. No significant increase of dispersion of bond lengths due to local compositional inhomogeneities caused by insertion of ZrO_2 into the CeO_2 lattice could be observed by EXAFS, when homogeneous systems (as above defined) were investigated [54].

The morphology of the powders is illustrated in Fig. 7 with some representative SEM micrographs. All micrographs were recorded on samples calcined at 500 °C. At low magnification it appears that all three powders have the same grain size dimension and morphology. This is an indication that the use of citrate synthesis methodology leads to comparable textural properties, independently of the sample composition. Accordingly, the different sintering behaviour of the samples should be mainly related to the effects of composition. As far as the porosity is concerned, the micrographs at higher magnification reveals the presence of porosity in the submicrometer range in CeO_2 and $Ce_{0.4}Zr_{0.6}O_2$ that is absent in pure ZrO_2.

4. Conclusions

The use of citrate complexation synthesis method allowed production of single phase $Ce_xZr_{1-x}O_2$ over a wide interval of compositions that feature consistent textural properties. This allowed the assessment of effects of composition on the textural and structural properties of these important catalytic materials. These findings can be summarised as follows: (i) sintering of the $Ce_xZr_{1-x}O_2$ particles strongly depends on the oxide composition, the lowest sintering rate being observed for intermediate composition; (ii) the sintering process significantly modifies the structure of solid solutions by creating a defective solid as more ZrO_2 is inserted into the CeO_2 lattice, provided that enough CeO_2 is present to avoid formation of the t-phase. Tetragonalisation of the lattice at high ZrO_2 contents can in fact release the lattice strain generated by the insertion of the small Zr(IV) cation in the lattice, leading to a less defective solid [9].

Defective structure has been shown to play a fundamental role in the catalytic properties of the CeO_2-based materials [49], accordingly a nano-sized defective CeO_2 oxide was significantly more active in redox catalytic reactions compared to conventional CeO_2 powders featuring larger particles [55]. On the contrary, as here observed, when the solid solution is sintered, due to the insertion of ZrO_2 into the CeO_2 lattice the structural and textural properties are remarkably modified with respect to CeO_2, since generation of defective structures is induced. This may explain some of the intriguing and unique properties of these catalysts such as the promotion of the reducibility at low temperatures, which can be induced by sintering at high temperatures [13,54,56].

Finally, the effects of the $Ce_xZr_{1-x}O_2$ composition on the sintering behavior suggest some possible guidelines for the choice of the appropriate composition to be employed in the catalytic application of these materials: due to the fast phase separation observed in the $Ce_{0.4}Zr_{0.6}O_2$ sample and the increase of BET area with CeO_2 content, cerium-rich compositions appear to be good candidates for low to medium temperature catalytic applications (< 1273 K). On the other hand when high temperatures are considered, ZrO_2-rich tetragonal phase could represent a good compromise due to its intrinsic thermodynamic stability coupled to a relatively small sintering rate, which allows a dispersed state of the

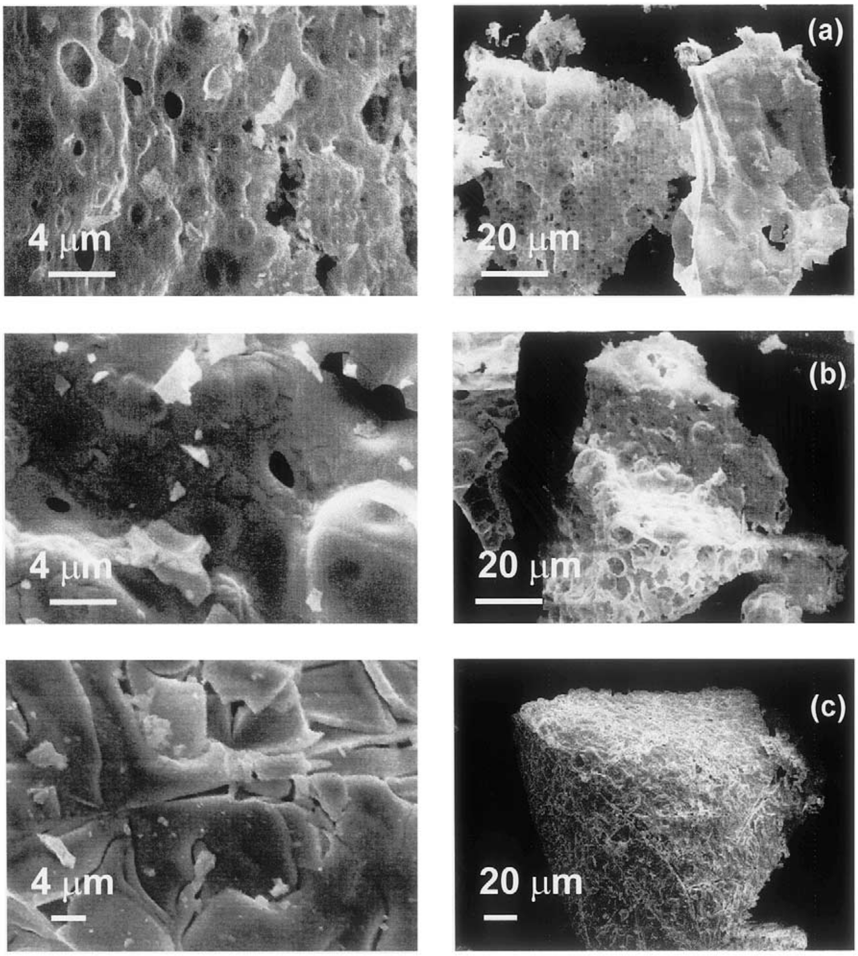

Fig. 7. SEM micrographs of (a) CeO_2, (b) $Ce_{0.4}Zr_{0.6}O_2$ and (c) ZrO_2.

catalyst to be maintained, even though the redox properties could be limited by the low cerium content.

Acknowledgements

The University of Trieste, Fondo Trieste 1999, MURST—PRIN 2000 'Catalysis for the reduction of the environmental impact of mobile source emissions', CNR Agenzia 2000, and project 'Urban Atmosphere'—Consortium INCA are gratefully acknowledged for financial support.

References

[1] J.M. Thomas, Angew. Chem., Int. Ed. 38 (1999) 3589.
[2] G.C. Bond, D.T. Thompson, Catal. Rev. Sci. Eng. 41 (1999) 319.
[3] M. Haruta, N. Yamada, T. Kobayashi, S. Iijima, J. Catal. 115 (1989) 301.
[4] M. Haruta, M. Date, Appl. Catal. A Gen. 222 (2001) 427.
[5] J. Kaspar, P. Fornasiero, M. Graziani, Catal. Today 50 (1999) 285.
[6] A. Trovarelli, Catal. Rev. -Sci. Eng. 38 (1996) 439.
[7] S. Bernal, J. Kaspar, A. Trovarelli (Eds.), Catal. Today, 20(2) (1999) 173.
[8] A. Trovarelli (Ed.), Catalysis by Ceria and Related Materials, vol. 2, Imperial College Press, London, 2002.
[9] P. Fornasiero, R. Di Monte, G. Ranga Rao, J. Kaspar, S. Meriani, A. Trovarelli, M. Graziani, J. Catal. 151 (1995) 168.
[10] H. Vidal, J. Kaspar, M. Pijolat, G. Colon, S. Bernal, A.M. Cordon, V. Perrichon, F. Fally, Appl. Catal. B Environ. 27 (2000) 49.
[11] H. Vidal, J. Kaspar, M. Pijolat, G. Colon, S. Bernal, A. Cordon, V. Perrichon, F. Fally, Appl. Catal. B Environ. 30 (2001) 75.
[12] P. Fornasiero, R. Di Monte, J. Kaspar, T. Montini, M. Graziani, Stud. Surf. Sci. Catal. 130 (2000) 1355.
[13] G. Balducci, P. Fornasiero, R. Di Monte, J. Kaspar, S. Meriani, M. Graziani, Catal. Lett. 33 (1995) 193.
[14] N. Izu, T. Omata, S. Otsuka-Yao-Matsuo, J. Alloys Comp. 270 (1998) 107.
[15] R.T. Baker, S. Bernal, G. Blanco, A.M. Cordon, J.M. Pintado, J.M. Rodriguez-Izquierdo, F. Fally, V. Perrichon, Chem. Commun. (1999) 149.
[16] T. Masui, T. Ozaki, K. Machida, G. Adachi, J. Alloys Comp. 292 (1999) L8.
[17] G.Y. Adachi, T. Masui, Synthesis and modification of ceria-based materials, in: A. Trovarelli (Ed.), Catalysis by Ceria and Related Materials, Chapter 3, Imperial College Press, London, 2002, pp. 51–83.
[18] T. Egami, W. Dmowski, and R. Brezny, SAE, 970461 (1997).

[19] S. Rossignol, F. Gerard, D. Duprez, J. Mater. Chem. 9 (1999) 1615.
[20] P. Fornasiero, G. Balducci, R. Di Monte, J. Kaspar, V. Sergo, G. Gubitosa, A. Ferrero, M. Graziani, J. Catal. 164 (1996) 173.
[21] A. Trovarelli, C. de Leitenburg, G. Dolcetti, Chemtech 27 (1997) 32.
[22] M. Fernandez Garcia, A. Martinez Arias, A. Iglesias Juez, C. Belver, A.B. Hungria, J.C. Conesa, J. Soria, J. Catal. 194 (2000) 385.
[23] J. Kaspar, R. Di Monte, P. Fornasiero, M. Graziani, H. Bradshaw, C. Norman, Top. Catal. 16 (2001) 83.
[24] P. Vidmar, P. Fornasiero, J. Kaspar, G. Gubitosa, M. Graziani, J. Catal. 171 (1997) 160.
[25] C. Marcilly, P. Courty, B. Delmon, J. Amer. Ceram. Soc. 53 (1970) 56.
[26] J.R. Anderson, K.C. Pratt, Introduction to Characterization and Testing of Catalysts, Academic Press, London, 1985.
[27] A.R. West, Basic Solid State Chemistry, 2, Wiley, Chichester, 1999.
[28] M. Yashima, H. Arashi, M. Kakihana, M. Yoshimura, J. Am. Ceram. Soc. 77 (1994) 1067.
[29] C.K. Narula, L.P. Haack, W. Chun, H.W. Jen, G.W. Graham, J. Phys. Chem. B 103 (1999) 3634.
[30] K. Otsuka, Y. Wang, M. Nakamura, Appl. Catal. A Gen. 183 (1999) 317.
[31] C.E. Hori, H. Permana, K.Y.S. Ng, A. Brenner, K. More, K.M. Rahmoeller, D.N. Belton, Appl. Catal. B Environ. 16 (1998) 105.
[32] C. Bozo, F. Gaillard, N. Guilhaume, Appl. Catal. A Gen. 220 (2001) 69.
[33] J.P. Cuif, G. Blanchard, O. Touret, A. Seigneurin, M. Marczi, E. Quémeré, SAE, 970463 (1997).
[34] J.P. Cuif, G. Blanchard, O. Touret, A. Seigneurin, M. Marczi, E. Quémeré, SAE, 961906 (1996).
[35] S. Meriani, Mater. Sci. Eng. A-Struct. Mater. 109 (1989) 121.
[36] S. Tsunekawa, R. Sivamohan, S. Ito, A. Kasuya, T. Fukuda, Nanostruct. Mater. 11 (1999) 141.
[37] R.D. Shannon, Acta Crystallogr. A32 (1976) 751.
[38] T. Moeller, in: J.C. Bailar, H.J. Emeleus, R. Nyholm, A.F. Trotmandickenson (Eds.), Comprehensive Inorganic Chemistry, Chapter 44, Pergamon Press, Oxford, 1982, p. 1.
[39] H. Cordatos, D. Ford, R.J. Gorte, J. Phys. Chem. 100 (1996) 18128.
[40] V.G. Keramidas, W.B. White, J. Am. Ceram. Soc. 57 (1974) 22.
[41] D.J. Kim, J.W. Jang, H.L. Lee, J. Am. Ceram. Soc. 80 (1997) 1453.
[42] T. Hirata, E. Asari, M. Kitajima, J. Solid State Chem. 110 (1994) 201.
[43] T. Hirata, J. Phys. Chem. Solids 56 (1995) 951.
[44] G.W. Graham, W.H. Weber, C.R. Peters, R.K. Usmen, J. Catal. 130 (1991) 310.
[45] M. Yashima, K. Ohtake, M. Kakihana, H. Arashi, M. Yoshimura, J. Phys. Chem. Solids 57 (1996) 17.
[46] T. Otake, H. Yugami, H. Naito, K. Kawamura, T. Kawada, J. Mizusaki, Solid State Ionics 135 (2000) 663.
[47] A.I. Leonov, A.B. Andreeva, E.K. Keler, Izv. Akad. Nauk SSSR, Neorg. Mater. 2 (1966) 137.
[48] G. Vlaic, R. Di Monte, P. Fornasiero, E. Fonda, J. Kaspar, M. Graziani, J. Catal. 182 (1999) 378.
[49] E. Mamontov, T. Egami, R. Brezny, M. Koranne, S. Tyagi, J. Phys. Chem. B 104 (2000) 11110.
[50] M. Maczka, E.T.G. Lutz, H.J. Verbeek, K. Oskam, A. Meijerink, J. Hanuza, M. Stuivinga, J. Phys. Chem. Solids 60 (1999) 1909.
[51] R.N. Blumenthal, J.E. Laubach, in: I.W. Vahlidick, S.A. Mersol (Eds.), Anisotropy in Single Crystal Refractory Compounds, Plenum, New York, 1968, pp. 137–150.
[52] G. Balducci, J. Kaspar, P. Fornasiero, M. Graziani, M.S. Islam, J. Phys. Chem. B 102 (1998) 557.
[53] G. Colon, F. Valdivieso, M. Pijolat, R.T. Baker, J.J. Calvino, S. Bernal, Catal. Today 50 (1999) 271.
[54] P. Fornasiero, E. Fonda, R. Di Monte, G. Vlaic, J. Kaspar, M. Graziani, J. Catal. 187 (1999) 177.
[55] A. Tschope, J.Y. Ying, Nanostruct. Mater. 6 (1995) 1005.
[56] S. Otsuka-Yao-Matsuo, N. Izu, T. Omata, K. Ikeda, J. Electrochem. Soc. 145 (1998) 1406.